Supersonic Conical Separation Due to Shock Vorticity

Frank Marconi*
Grumman Aerospace Corporation, Bethpage, New York

A numerical study of the conical, supersonic, inviscid flow about circular slender cones at large incidence is presented. Although the flow is assumed inviscid, separation and an accompanying spiral are found. This phenomenon is shown to be a valid solution to Euler's equations, i.e., valid in the sense of being independent of any numerical viscosity. The separation and spiral are caused solely by the vorticity produced by a cross-flow shock. The resulting separated flowfields are compared to full potential calculations and to experimental data.

Introduction

THREE-DIMENSIONAL separated flows are, in general, accompanied by the spiraling of streamlines into a vortex. The phenomenon is important in many flow situations: the flow about the leading edge of a wing; the flow behind bluff bodies; and the flow on the lee side of slender bodies at large angles of attack. The control of vortices for increased aerodynamic efficiency has been studied by aircraft designers for many years and was the subject of a recent paper by Rao.[1] The current paper is a numerical study of spiraling vortex flow about slender cones flying at supersonic speeds and large incidence. Although the cones considered here may be slender, the full inviscid Euler equations are solved. An understanding of these flowfields has direct applicability to missile aerodynamics and to the aerodynamics of aircraft forebodies.

All geometries considered in this numerical study are circular cross-section cones, so that while the flow is in a real sense three-dimensional, all flow variables depend on only two coordinates. The flowfield is assumed supersonic everywhere and conical. In addition, the gas is assumed ideal with a ratio of specific heats of 1.4 (i.e., air). It should be realized that while the assumption of conical flow does simplify the numerical problem, the conclusions reached have more general applicability. The basic features of the flowfield are essentially unchanged in the fully three-dimensional flow.

Conical streamline spirals occur in the separation region on the leeward side of slender cones at large angles of attack (see Figs. 1 and 2). The existence of this type of flow pattern in purely inviscid flow has been the subject of study for many years. Küchemann[2] proved analytically that for two-dimensional flow with distributed vorticity, inviscid separation can occur. Two-dimensional flow separation is accompanied by a closed recirculation zone. The streamlines "trapped" inside this recirculation zone cannot be tracked back upstream where all flowfield conditions are known. Flow properties that are transmitted along streamlines (for example, entropy and vorticity) must somehow be determined inside the closed recirculation zone. Fraenkel[3] found closed-form solutions for the incompressible two-dimensional flow over cylinders with closed recirculation zones caused by distributed vorticity in the freestream. Smith[4] used the analytical work of Küchemann to numerically compute recirculation zones at the trailing edge of a two-dimensional airfoil. The vorticity in this case was imposed at a finite distance upstream of the trailing edge. This situation is similar to vorticity being generated by a transonic shock near the trailing edge of an airfoil. More recently, a number of researchers working on solutions to Euler's equations in two-dimensional transonic flow[5,6] have found inviscid separation and recirculation zones behind cylinders and airfoils. Salas[5] showed how Euler solutions with transonic shocks can exhibit recirculation zones behind cylinders. The vorticity and entropy trapped in the recirculation zone are said to be determined by the time-dependent computation used to asymptote to a steady solution.

In fully three-dimensional flow and the conical flows considered here, separation is not accompanied by a closed recirculation zone but by spiraling streamlines.[7] This point is important because in the conical flow all streamlines originate in the freestream where all flowfield quantities are known. Therefore, entropy and vorticity can be uniquely determined everywhere, along with the flowfield and, in particular, the required shock system. Figure 1 shows a three-dimensional surface streamline starting from the windward plane wetting the body surface and getting swept up into the spiral. Figure 2 is a sketch showing how the cross-flow streamlines, which start outside the bow shock, pass through the shock system, and ultimately get swept up into the spiral singularity or a lee plane node (Fig. 2b). The dashed line of Fig. 2b divides the flow that is swept into the spiral node from that which goes into the lee plane node. Cross-flow streamlines are defined as the intersection of fully three-dimensional stream surfaces and the surface of a sphere centered at the apex of the cone. Their direction in the x-y plane (Fig. 2) can be defined as the ratio of the two components of the cross-flow velocity u and v (Fig. 1).

In the current paper, separation will be loosely defined as the process by which a stream surface originally on the cone leaves the cone surface and ultimately forms an infinitely turning spiral (see Figs. 1 and 2). Separation occurs along a line in conical flow; the intersection of this line and the cross-flow plane will be referred to as the separation point. In a review paper on conical streamline singularities, Smith[9] showed analytically that a conical spiral singularity can exist only in flows with vorticity. In particular, he found that a finite radial (spherical r, Fig. 1) component of vorticity was a necessary while not sufficient condition for the existence of a spiral. It seems clear that separation and an accompaning spiral are linked to the generation of vorticity and not to the details of the viscous processes involved.

There are three ways of introducing vorticity in an otherwise irrotational flow: 1) by specifying vorticity in the freestream, as was done in Refs. 3 and 4; 2) through shock waves; and 3) by shedding vorticity from the boundary layer at a separation point. In this paper only the vorticity produced by the shock system will be discussed in detail. It should be noted that currently only through solutions of the Euler

Presented as Paper 83-1665 at the AIAA 16th Fluid and Plasma Dynamics Conference, Danvers, Mass., July 12-14, 1983; submitted July 30, 1983; revision received Nov. 18, 1983.

*Senior Staff Scientist, Research and Development Center. Member AIAA.

equations can this aspect of the flow be modeled (i.e., full potential shocks do not generate vorticity). The third mechanism of vorticity introduction, shedding, has been studied extensively by Smith[9-10] and Fiddes.[11] The current author has shown preliminary Euler solutions that use this model to force separation at a specified location.[12]

In order to shed vorticity, the flow is modeled by assuming that there exists an infinitesimally thin sheet of infinite vorticity across which there is a jump in velocity. The rest of the flow can be assumed irrotational. The vortex sheet will generally roll up into a spiral. The sheet is forced to originate at a separation point by imposing a Kutta condition. At sharp edges (sharp wing tip, for example), the condition is similar to that imposed at wing trailing edges in three-dimensional flow to exclude singularities due to flow turning around sharp edges. For smooth bodies, the proper Kutta condition to be imposed to start a vortex sheet in an otherwise completely irrotational flow has been studied in detail in Refs. 9 and 10. The location of the origin of shedding on the body is the only free parameter and is specified to match the boundary-layer separation point. In contrast to bodies with salient edges, where the edge is taken as the separation point, smooth bodies require that the separation point be computed from a boundary layer coupled to an inviscid flow iteration[11] or from experimental data. Calculations including forced separation from a shedding vortex sheet have been performed for a number of years (for example, the early work of Bryson[13]). More recently, Rizzi[14] has shown solutions to Euler's equations with separation from sharp leading edge wings, and Nielsen[15] has shown solutions to Euler's equations with separation from smooth bodies. It should be pointed out that the work of Refs. 14 and 15 seem inconsistent with the analysis of Refs. 9 and 10 for the flow near the origin of this sheet (i.e., the separation point), while the present author has used the model of Ref. 9 to force separation at a specified location.[12]

It should be made clear at this point that the two mechanisms of vorticity introduction, shock waves and shedding, both produce valid solutions to Euler's equations with separation and spirals. While the two mechanisms produce similar flowfield structures, the details of the separation and spiraling sheet are different. The differences in detail are outlined in Ref. 12. The main difference should be clear. The separation caused by the shock vorticity occurs with no additional conditions and uniquely determines separation point location, while the forced separation point location is arbitrary. It is the arbitrariness of the separation point location that allows the freedom necessary to match the boundary-layer separation point location. The separation point in the shock-induced case may bear little relation to the real viscous flow, but the shock-produced vorticity can play a role in the structure of the real separated flow. The point here is that the vorticity in the flowfield comes from two sources—shock waves and shed from the boundary layer—both of which contribute to the quantitative structure of the flow. Only the shock vorticity will be considered herein, so it is not surprising that the comparisons with experimental data are poor in some sense; in particular, the separation point locations are significantly different.

The intent of this paper is to show that the vorticity produced by shock waves can cause separation and that solutions to the inviscid Euler equations exhibiting this phenomenon are valid, in the sense of being independent of any numerical artifices. The qualitative structure of the separated flow produced by shock vorticity will be shown to be the same as that produced in the presence of a boundary layer, indicating the possibility of this vorticity being significant. In the section that follows, the overall computational procedure will be outlined. The issues of convergence both in terms of iteration scheme and grid refinement will be addressed in this section. Then a detailed study of computational results will be presented including comparisons with experimental data and full potential calculations. The final section of the paper will present a summary of the findings of this work and the future directions of this effort.

Computational Procedure

The overall numerical procedure used in this study, although employing a number of new features, is essentially standard.[16] The fully three-dimensional Euler's equations are solved with an explicit marching technique. The marching direction (z, Fig. 1) is an iterative coordinate for the conical flow considered here. The scheme is restricted by the fact that the axial component of velocity (W, Fig. 1) must be supersonic everywhere. The marching scheme is continued until the flowfield is invariant with respect to the computational marching direction except for a scale factor. The finite-difference scheme used is Moretti's characteristic based λ-scheme.[17] All shock waves in these flowfields are fit and are forced to satisfy the exact Rankine-Hugoniot jump conditions. The bow shock is fit as the outermost boundary of the flowfield. On the low pressure side of the bow shock, freestream conditions exist. The cross-flow shock is fit as an internal boundary of the flowfield with its low pressure side being computed as the computation proceeds.[18]

The cross-flow shock computation is a critical part of the overall procedure, particularly since it plays such a critical role in separation. As mentioned in the previous section, it is the vorticity produced by the cross-flow shock that produces the spiral. Any scheme that captures the cross-flow shock and introduces additional artificial viscosity to stabilize it runs the risk of distorting the separation and spiral. The bow shock

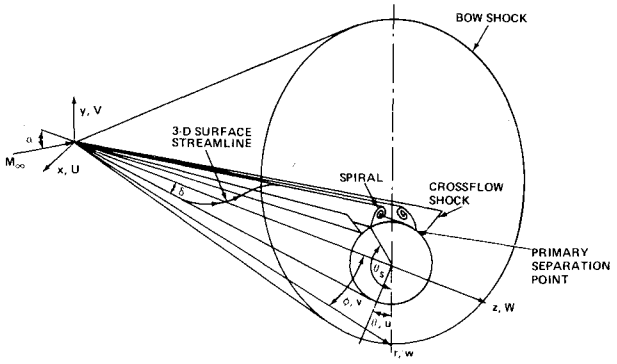

Fig. 1 Three-dimensional sketch of flowfield and coordinate system.

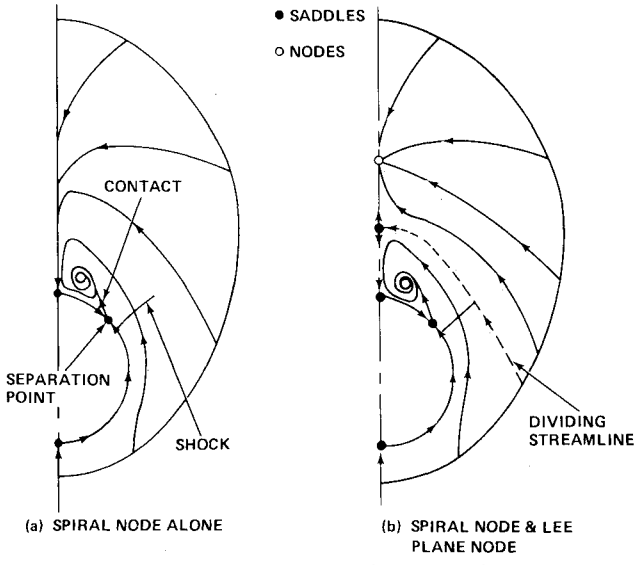

Fig. 2 Sketch of cross-flow streamlines.

also introduces vorticity in the flowfield, but not enough to produce separation. The cross-flow shock is caused by the fact that at a large incidence the θ component of the velocity (u, Fig. 1) becomes supercritical. The flow expands in going from the windward symmetry plane, and u can become supercritical if the incidence is high enough. This component of velocity must vanish in the lee symmetry plane due to the boundary conditions. A supercritical cross flow generally passes through a relatively normal shock before stagnating in the lee plane. The cross-flow shock exists to turn the three-dimensional flow parallel to the lee symmetry plane. The variation in strength of the cross-flow shock can be quite large. The shock is strongest at the body where u is highly supersonic and approaches zero strength in the field where u becomes sonic. It is this variation in strength that produces a cross-flow entropy gradient and thus radial vorticity. This vorticity, in turn, causes shock-induced separation.

The low-pressure side of the cross-flow shock is computed with one-sided differences away from the shock. This is consistent with the fact that the cross flow is supersonic. The Rankine-Hugoniot conditions and the compatibility condition along a bicharacteristic reaching the shock on its high-pressure side supply enough information to compute the deviation of each shock point from a conical ray in addition to all the primitive variables on its high-pressure side. The bicharacteristic used is the one in the plane containing the local normal to the shock and the marching direction. All shock points are computed with the postcorrection scheme proposed by Rudman[19] and independently by deNeef.[20] The shocks converge (i.e., each shock point becomes aligned with a conical ray) with the rest of the flowfield. In all the computations presented here, the last cross-flow shock point fit had a normal Mach number of about 1.05 (pressure ratio of 1.12). The finite difference scheme was able to capture weaker shock points.

An exponential stretching is used to cluster grid points near the surface of the cone. This is important because flow conditions that exhibit the spiral singularity also exhibit large gradients near the body behind the cross-flow shock. Without the stretching, the radial resolution behind the shock can be too coarse to pick up the separation and spiral (see, for example, the Euler calculations made using a procedure very similar to the one used here without a stretching present in Ref. 21). The stretching is of the form:

$$\bar{r} = -\ell n(1-(1-e^{-\beta})X)\,(C-B)/\beta + B \qquad (1)$$

where $\bar{r}$ is the polar radius in the x-y plane (not to be confused with the spherical radius r of Fig. 1), and X is the computational coordinate going from 0 on the body to 1 at the bow shock. The other computational coordinate is Y, which is a linearly normalized polar angle θ. Y is normalized to go from 0 in the windward symmetry plane to 1 on the low-pressure side of the cross-flow shock and from 0 again on the high-pressure side of the shock to 1 in the lee plane. The transformation to the final computational plane is completed by $Z=z$. In the transformation, Eq. (1), B and C are the polar radii of the body and bow shock, and β is a clustering parameter. The grid points are evenly spaced in each X-Y plane. The transformation, Eq. (1), clusters grid points near the body depending on the value of β used. The transformation approaches linear as β goes to zero. All of the calculations shown here were performed with $\beta=2.5$. The gradient in the strength of the cross-flow shock is quite large, which is the reason for the large vorticity produced behind it. The clustering of grid points near the body allows for enough resolution to compute this shock decay properly. The number of points required to resolve this phenomenon without a stretching would be inordinately large.

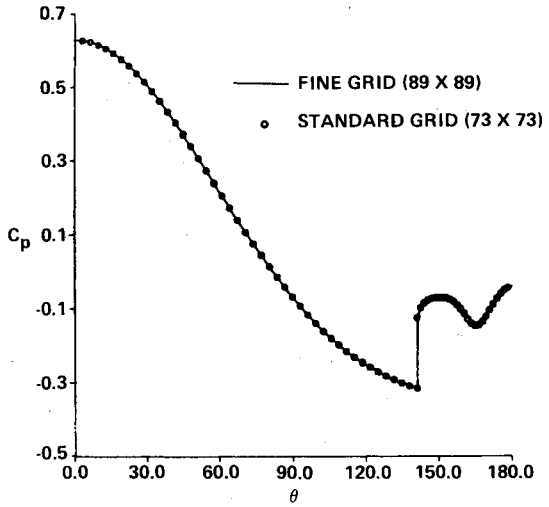

Fig. 3 Comparison of computation with two grids, surface pressure ($M_\infty=2$, $\delta=10$ deg, $\alpha=25$ deg).

Shock-induced inviscid separation produces a contact surface emanating from the separation point (Fig. 2). It is this contact that ultimately spirals. The contact surface has a jump in entropy and an accompanying jump in velocity. In conical flow, entropy is constant on cross-flow streamlines. With this fact, one can see (Fig. 2) that the entropy on the wind side of the contact comes from the wind symmetry plane bow shock. The streamline wets the body and passes through the base of the cross-flow shock. This is the high entropy side of the contact. There are two possibilities for the entropy on the lee side of the contact. The one shown in Fig. 2a corresponds to the lee bow shock entropy wetting the lee side of the cone and ending up on the lee side of the contact. There is a possibility of a saddle point existing in the lee symmetry plane off the body as shown in Fig. 2b. In this case, the entropy on the lee side of the contact would come from this saddle. In either case the cross-flow steamlines that wet the body are tracked in each step of the iteration, and the proper entropy is imposed on the cone including the jump in entropy at the separation point. The entropy discontinuity off the body is captured with the finite difference scheme.

The finite difference scheme[17] used requires that all spatial differences (computational X and Y) be directional, depending on characteristic directions. In the case of entropy, the characteristic direction is the particle path or streamlines, so that both X and Y derivatives of entropy are taken depending on the direction of the local flow. The scheme basically avoids differences across the contact. In order to achieve formal, second-order accuracy, the λ-scheme uses three-point, one-sided differences. In this flowfield, the three-point differences in entropy sometimes required crossing the contact, which caused wiggles. In order to ensure monotonicity at the sheet, these differences in entropy were taken with two-point windward formulas. The sheet was captured between two points until it began to roll up. The region where the sheet rolls up is somewhat smeared, but the scheme seems to describe this region adequately. In any inviscid calculation, approximations must be made for the region near the center of the spiral. In the irrotational calculations of Refs. 11 and 13, the center of the spiral is replaced by a concentrated vortex. One advantage of solving the Euler equations is that this region of concentrated vorticity can be computed automatically.

It was proven by Smith[9] that a forced sheet leaves a smooth body tangent to the surface and that there must be a jump in cross-flow velocity at separation. The cross-flow velocity on the windward side of the sheet is finite, while the cross flow on the lee side stagnates. The arguments of Ref. 9 are based on irrotational and isentropic assumptions and do not hold for flows with cross-flow shocks. It can be shown that when the sheet exhibits a jump in entropy, the cross-flow velocities on either side of the sheet can match and still maintain con-

tinuous pressure across the sheet. Of course the modulus of the velocity must then jump. This jump is absorbed in the radial component of velocity (w, Fig. 1). This seems to be the situation in the inviscid shock-induced separation. Results will be shown later that indicate the continuous variation of cross-flow through the separation point for the shock-induced case.

In order to speed convergence, grid refinement was used in all the calculations shown in this paper. The calculations were started with a 10×10 (polar radial x circumferential) grid. The calculation was continued until a reasonable convergence was reached, and then the grid was halved. The grid was refined three times, the final grid having 73×73 points in each X-Y plane. The iteration was continued on the finest grid until the maximum variation in pressure in the spherical radial (r, Fig. 1) direction was less than 1×10^{-7}. This is the maximum correction in pressure. The solutions are essentially converged at a maximum correction of 10^{-5} so that 10^{-7} is a conservative convergence criterion. This is a reduction of about nine orders of magnitude from the beginning of the iteration. Critical parameters such as shock location and stagnation point location are constant to five places by the time the calculation is stopped.

The sensitivity of this calculation to the initial conditions used was studied early in this work. It was found that the captured shock, coarse grid, initial conditions to the fine grid exhibited a spiral. The spiral was eliminated before starting the shock fit, fine grid calculations with no change in the final result. The spiral simply developed again. In a numerical experiment, a converged high α (with spiral) result was used as initial condition for an $\alpha=0$ case. The incidence was reduced gradually, and the cross-flow shock was weakened and ultimately was eliminated along with the spiral. The opposite sequence was tried and the spiral reappeared. The numerical experiments indicated an independence of the converged solution to initial conditions.

The finite difference scheme used in this work is an explicit marching scheme that is notoriously inefficient for converging to a conical or steady solution. A number of speed-up procedures were tried, including multigrid and local marching steps.[5] None of these worked. Local marching steps did produce a significant reduction in running times, but proved unstable in the presence of the cross-flow shock. The cross-flow shock was captured with the λ-scheme in the first two coarse grid calculations. The shock was detected and fit from the third grid on. While the captured shock location was significantly off the converged result, this scheme eliminated some shock detection problems. One advantage of the explicit marching scheme used was that it is totally "vectorizable." The time consuming parts of the code (i.e., interior point computation) utilized the vector architecture of the CRAY 1 computer. This made the computation about 20 times faster on the CRAY than on an IBM 3033. All the computations shown in this report took about 30 CPU minutes on the CRAY 1.

Figure 3 shows a comparison of the surface pressure for the flowfield about a 10 deg half-angle cone at $M_\infty=2$ and $\alpha=25$ deg. The symbols are the pressure computed with the standard 73×73 grid. The solid line was computed with a finer 89×89 grid. The figure shows that the fine and standard grid surface pressures are virtually identical, indicating that the standard 73×73 grid resolves all flowfield features. In both calculations, about 35% of the circumferential points are behind the cross-flow shock (i.e., 27 points for the 73×73 grid). This flowfield has a shock-induced separation at $\theta=149.6$ deg, indicated by the minimum in surface pressure behind the shock ($\theta\approx165$ deg). This minimum in pressure is just below the core of the spiral. Both computations, 73×73 and 89×89, give the same separation point and spiral location, indicating an independence of the results to numerical viscosity due to truncation error. As a matter of fact, this flowfield was computed with an even coarser grid (37×37) that exhibits the same basic features (i.e., separation and spiral). While it is very difficult to prove the existence of shock-induced inviscid separation, the aforementioned numerical experiments indicate the validity of such solutions. Additionally, the analytical work for two-dimensional flow reported in Refs. 2 and 3 confirm the possibility of such solutions. The uniqueness of the conical flow solution would seem to be on firmer ground because of the absence of closed recirculation zones.

Computational Results

In this section, computational results showing spiraling streamlines due to the vorticity produced by a cross-flow shock will be analyzed. The first configuration considered is a 10-deg cone at $M_\infty=2$ and $\alpha=25$ deg. The surface pressure distribution has been shown in Fig. 3. The cross-flow streamlines are shown in Fig. 4, along with the computed bow and cross-flow shocks. The streamlines show saddles in the wind and lee symmetry planes on the cone surface. In addition, there is a saddle at the separation point and a node at the center of the spiral (this configuration is sketched in Fig. 2a). The separation point and spiral can be seen more clearly in the blowup of Fig. 5. If the nodes and saddles are summed using the procedure of Ref. 8, it can be shown that the proper number of nodes and saddles exist in the streamline pattern of Fig. 4. The separation point ($\theta_s=149.6$ deg) corresponds to

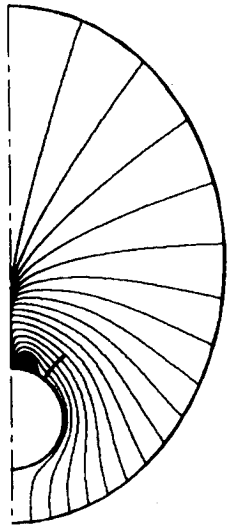

Fig. 4 Cross-flow streamlines in field ($M_\infty=2$, $\delta=10$ deg, $\alpha=25$ deg).

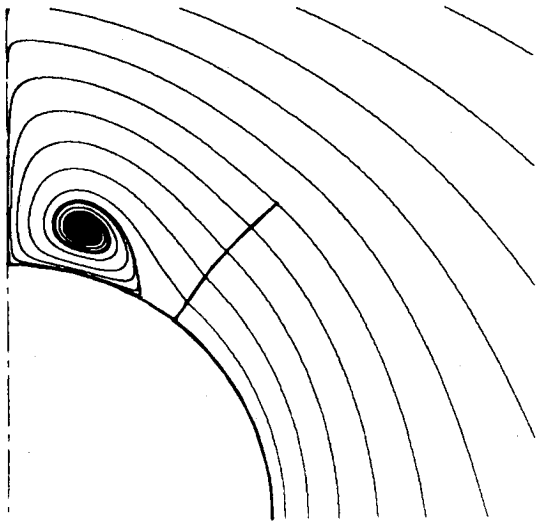

Fig. 5 Cross-flow streamlines near lee plane ($M_\infty=2$, $\delta=10$ deg, $\alpha=25$ deg).

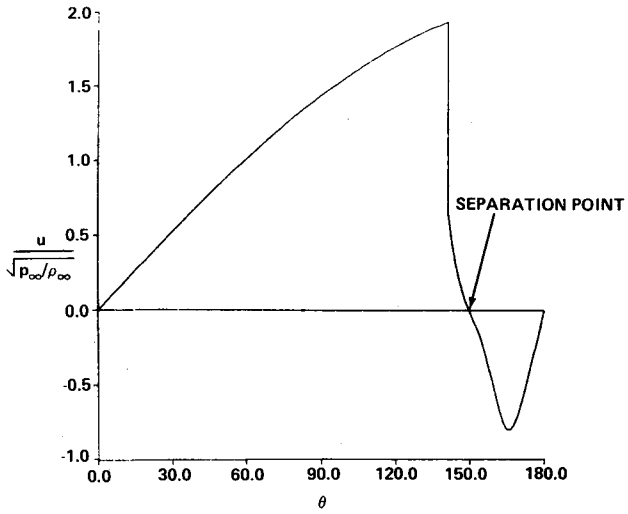

Fig. 6 Surface cross-flow velocity ($M_\infty = 2$, $\delta = 10$ deg, $\alpha = 25$ deg).

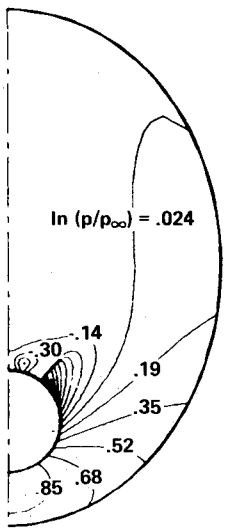

Fig. 7 Isobars in cross plane ($M_\infty = 2$, $\delta = 10$ deg, $\alpha = 25$ deg).

the plateau in pressure (Fig. 3) just after the shock. If one considers the momentum equation in the θ direction, it indicates that $\partial p/\partial\theta = 0$ at a cross-flow stagnation point ($u = v = 0$). The separation point in this flowfield is a real cross-flow stagnation point. The streamlines (Fig. 5) show that the flow moves in the negative θ direction from the lee stagnation point toward the separation point. In doing so, the flow expands (i.e., drop in pressure between $\theta = 180$ deg and $\theta = 165$ deg). The flow then recompresses to the separation point. This recompression phenomenon is the cause of secondary separation. The inviscid separation point location is far from that of the viscous flow. This can be surmised by the fact that the shock is strong enough to separate a boundary layer at its base. The inviscid separation point is too far downstream of the shock. The streamlines of Fig. 5 clearly show how all of the flow is ultimately swept up into the infinitely turning spiral. The apparent power of the Euler equations to describe the region near the center of the spiral should be noted. A detailed study of the streamline pattern near the center of the spiral revealed that the streamlines asymptote to an ellipse. This was first indicated by Smith.[9] It also should be pointed out that Fig. 5 shows that streamlines wrapping around the spiral very rapidly approach the lee side of the separation line (contact). Consider, for example, the third streamline off the cone in Fig. 5. It wraps around the top of the spiral, comes back, and approaches the contact a short distance off the body, creating an entropy layer on the lee side of the contact. This entropy layer tends to weaken the contact.

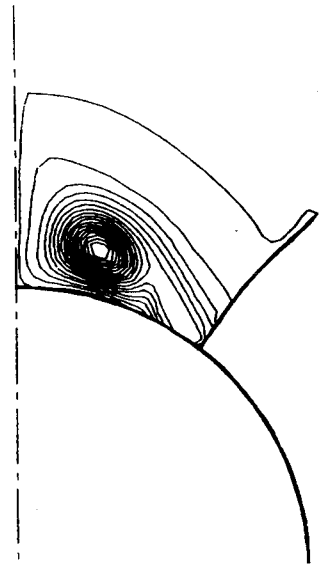

Fig. 8 Lines of constant radial vorticity × spherical radius ($M_\infty = 2$, $\delta = 10$ deg, $\alpha = 25$ deg).

Figure 5 also shows that the separation line leaves the cone at a finite angle. Smith's analysis[9] concluded that at a forced separation the sheet comes off tangent. However, this difference is due to the fact that the separation in the shock-induced case is nonisentropic and is a real cross-flow stagnation point. Figure 6 shows the cross-flow velocity on the surface of the body ($v = 0$ from the body boundary condition). The point to be considered here is that the velocity passes through zero (separation) smoothly. The analysis of Smith indicates that separation occurs at a discontinuity in cross flow, the jump in velocity determining the sheet strength. This is a basic difference between forced and shock-induced separation and is discussed in detail in Ref. 12. The jump in cross-flow velocity in Fig. 6 is due to the shock. It is also interesting to note the maximum negative u that occurs under the spiral. This negative cross flow can become supersonic, causing a second reverse cross-flow shock. A sample of this will be shown later.

Figure 7 shows the isobars for the same case ($M_\infty = 2$, $\delta = 10$ deg, $\alpha = 25$ deg). It should be noted how smoothly the cross-flow shock transitions to zero strength in the field. The most interesting aspect of the figure is the closed isobar at the center of the spiral. It represents an absolute minimum in the flowfield pressure. The component of vorticity in the spherical radial direction is given by:

$$\Omega_r = -\left(u\cos\phi + \frac{\partial u}{\partial\phi}\sin\phi - \frac{\partial v}{\partial\theta}\right)\Big/(r\sin\phi)$$

where u and v are the cross-flow velocities defined in Fig. 1 and r, θ, ϕ are spherical coordinates (Fig. 1). Figure 8 shows lines of constant $r\Omega_r$. The figure shows how the vorticity is distributed and is produced by the cross-flow shock. Note that Ω_r is small until the cross-flow shock, indicating that the bow shock doesn't produce enough vorticity to cause separation on its own. The vorticity produced by the bow shock is an order of magnitude smaller than that produced by the cross-flow shock and two orders of magnitude smaller than that at the center of the spiral. For this reason, there are no contours of vorticity outside the region behind the cross-flow shock in Fig. 8. The vorticity is negative causing the counterclockwise spiraling of this flow, and its absolute magnitude is maximum at the center of the vortex.

The results shown in Figs. 9-11 are all for the same flow conditions ($M_\infty = 2$, $\delta = 10$, $\alpha = 20$ deg). This is a lower angle of attack than the previous case, so that the spiral is smaller

and has moved toward the lee plane. This can be seen by comparing Figs. 5 and 10. It also can be seen from the streamlines (Figs. 9 and 10) that this configuration has an additional saddle/node combination in the lee plane as sketched in Fig. 2b. The dashed line ending at the saddle in the lee plane divides the flow, which is ultimately swept into the spiral node from that which ends up in the node in the lee symmetry plane. The entropy on the dashed streamline ultimately wets the lee side of the contact (separation line). This type of structure has been noticed experimentally.[22] The phenomenon is similar to the standard "liftoff" conical flow structure noticed at lower incidence with no spiral. In the present study, subcritical incidences were computed for the same 10-deg cone at $M_\infty = 2$, and liftoff was observed with no vortex. As the incidence is raised, the flow becomes supercritical and the spiral begins to form near the lee plane. The liftoff remains, as shown in Figs. 9 and 10. As the incidence is raised still further, the spiral gets larger and the liftoff is eliminated (see Figs. 4 and 5). It should be noted that the limiting streamline (dashed line in Fig. 10) seems not to approach the saddle normally. This is possible if distributed vorticity is present in the flow,[23] which is the case here. The isobars in Fig. 11 show that the vortex is so weak that the minimum in pressure at its center does not appear due to the resolution of the contours.

Figure 12 is a plot of the inviscid separation point location vs a measure of shock strength. The cone has a 10-deg half-angle and the freestream Mach number is 2. The cross-flow shock strength was increased by increasing incidence. The pressure ratio used is the one at the base of the shock; of course, all cross-flow shocks go to zero strength at their tips. The pressure ratio used is a good measure of the shock strength variation and thus the vorticity produced by the shock. At each data point, the corresponding α is noted. The plot shows how as the shock strength decreases, the separation point moves to the lee symmetry plane. At the same time, the spiral region is getting smaller. The highest incidence computed was 25 deg, since above that value the axial Mach number on the cone surface approaches sonic, making it impossible to march. At the low end, $\alpha = 19$ deg, the spiral was so small that it was difficult to resolve numerically, and no lower incidences are shown. The interesting feature of this figure is that an extrapolation of the curve would seem to indicate that inviscid separation moves to the lee plane before the shock is eliminated ($p_2/p_1 = 1.$). An extrapolation would indicate that the spiral is eliminated at $p_2/p_1 \approx 1.85$. This corresponds to a normal Mach number slightly above 1.3, which is approximately the region where the full potential

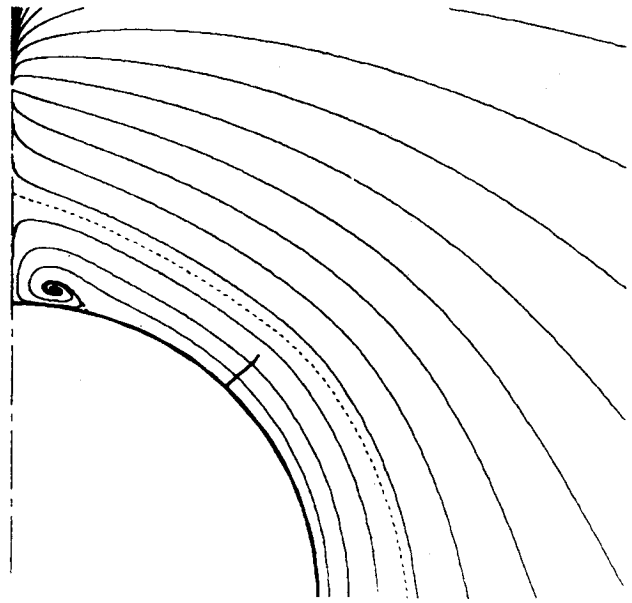

Fig. 10 Cross-flow streamlines near lee plane ($M_\infty = 2$, $\delta = 10$ deg, $\alpha = 20$ deg).

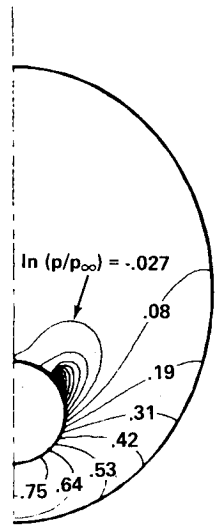

Fig. 11 Isobars in cross plane ($M_\infty = 2$, $\delta = 10$ deg, $\alpha = 20$ deg).

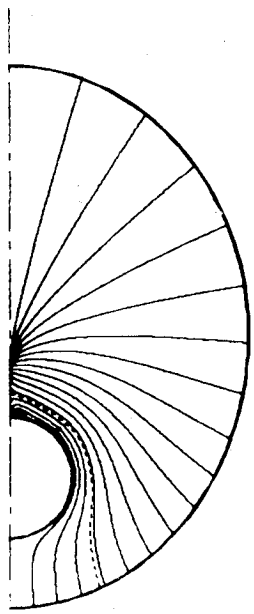

Fig. 9 Cross-flow streamlines ($M_\infty = 2$, $\delta = 10$ deg, $\alpha = 20$ deg).

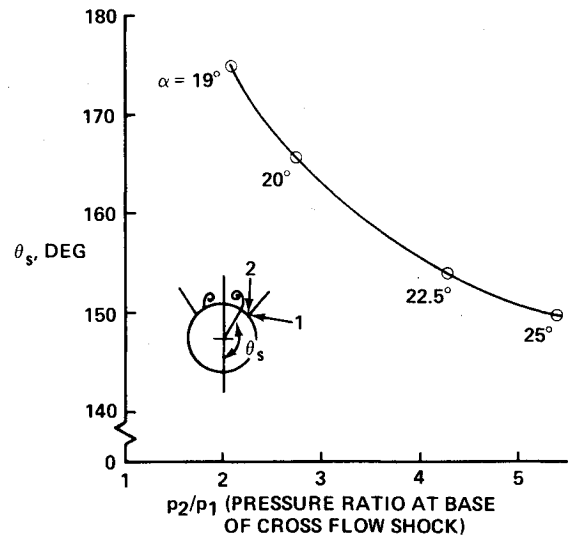

Fig. 12 Inviscid shock-induced separation point location vs shock strength ($M_\infty = 2$, $\alpha = 20$ deg).

approximation is valid for these flowfields. It would seem that below a maximum normal Mach number of 1.3, the cross-flow shock may not produce enough vorticity to cause separation.

Figures 13-15 deal with an interesting case ($M_\infty = 3$, $\delta = 9.46$ deg, and $\alpha = 25$ deg). Figure 13 show the streamlines and the cross-flow shock near the lee plane. The shock exhibits a kink as it passes from the influence of the spiral. Near the cone, the shock must deflect the streamlines upward in order that they may pass over the spiral; beyond the top of the spiral, this is no longer true and the shock acts like a normal shock. The two regions are separated by the kink in the shock, and the shock slope in the cross-flow plane had to be differenced away from this point. Another interesting feature of this flow is the fact that the expansion of the reverse flow from the lee stagnation point is so large that the negative cross flow becomes supersonic near the body. The smooth recompression shown in Fig. 3 is replaced by a reverse cross-flow shock. This phenomenon has been noted experimentally in Ref. 24. The reverse cross-flow shock, which was captured, can be seen in the isobars of Fig. 14. The second (reverse) shock is on the lee side of the primary cross-flow shock. It is indicated by the clustering of the isobars between $\ln(p/p_\infty) = -1.2$ and $\ln(p/p_\infty) = -0.73$ on the cone surface. The shock is not strong enough to produce a secondary inviscid separation, whereas in the experiment of Ref. 24 it was strong enough to separate the boundary layer. The possibility of having secondary separation produced solely by shock vorticity is an interesting topic for future study. The strength of the vortex is also indicated in Fig. 14 by the closed isobars representing a steep pressure minimum at the vortex center.

Figure 15 shows the surface pressure for the $M_\infty = 3$, $\delta = 9.46$ deg, and $\alpha = 25$ deg case. The solid line is the present calculation with shock vorticity-induced separation at $\theta = 155.3$ deg, again at the plateau in pressure just after the primary cross-flow shock. The reverse cross-flow shock can be seen in the pressure distribution at about $\theta = 167$ deg. The shock is captured, and so it is smeared over a mesh interval. The figure also shows the numerical results of Ref. 15. They are also a solution to Euler's equations but with the primary cross-flow shock was captured. In the results of Ref. 15, the separation point was forced to occur at $\theta = 120$ deg in order to match the boundary-layer separation point found experimentally. The forced separation model of Ref. 15 is in contradiction to the analytical work of Smith.[10] In addition, there are anomalies in the results of Ref. 15. Basically the comparison of Fig. 15 shows that the two results are very close, while the separation points are very different. It seems that forcing separation at $\theta = 120$ deg simply inserted a wiggle

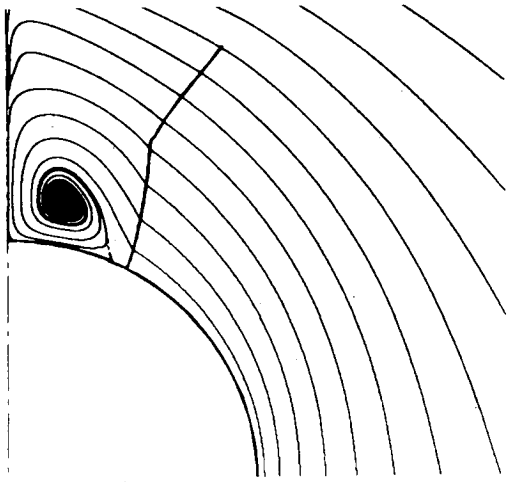

Fig. 13 Cross-flow streamlines near lee plane ($M_\infty = 3$, $\delta = 9.46$ deg, $\alpha = 25$ deg).

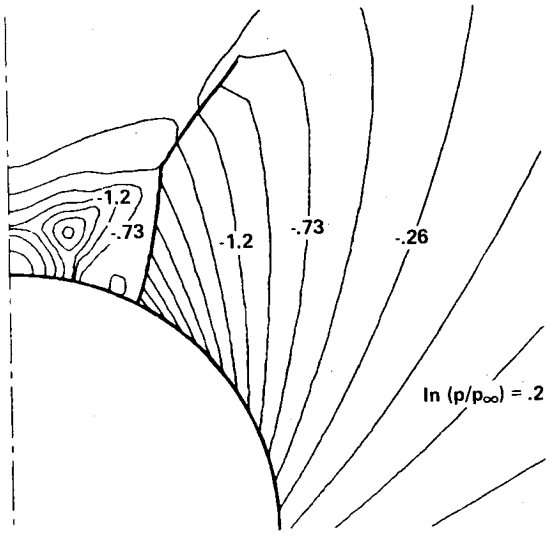

Fig. 14 Isobars near lee plane ($M_\infty = 3$, $\delta = 9.46$ deg, $\alpha = 25$ deg).

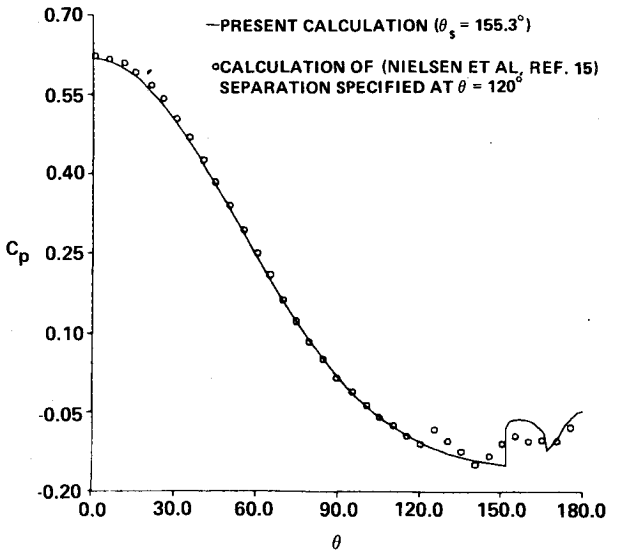

Fig. 15 Surface pressure comparison ($M_\infty = 3$, $\delta = 9.46$ deg, $\alpha = 25$ deg).

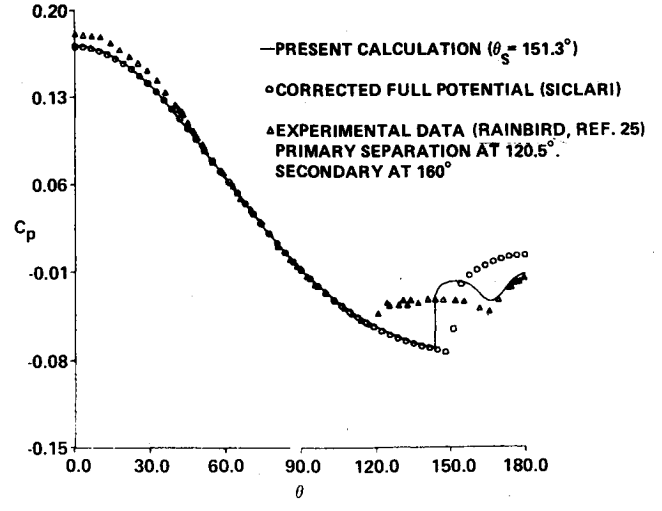

Fig. 16 Surface pressure comparison ($M_\infty = 4.25$, $\delta = 5$ deg, $\alpha = 25$ deg).

in the surface pressure distribution of Ref. 15. The flow then came back to the shock-induced flowfield. The cross-flow shock locations are very close. The shock of Ref. 15 is smeared over a few points but is close to the fit shock of the present calculations. If separation did occur at 120 deg, there must be a cross-flow shock before $\theta = 120$ deg. However, there is no evidence of a shock before separation in the results of Ref. 15.

Figure 16 shows the pressure distribution on a 5-deg cone at $M_\infty = 4.25$ and $\alpha = 12.35$ deg. Compared are the results of the present calculation, those computed using the full potential equation supplied by Siclari, and the experimental results of Rainbird.[25] The potential results of Siclari have been corrected for nonisentropic bow shock effects while maintaining the irrotational assumption. Figure 16 indicates that the Euler and potential results are virtually identical until the shock. The potential result does not exhibit the minimum in pressure behind the shock typical of separation. Potential calculations cannot predict separation or spiraling without a shedding sheet. The comparison between Euler and potential calculations affirms the fact that rotationality is important only after the cross-flow shock. A comparison between the present calculation and the experimental results of Rainbird clearly shows that the vorticity produced by the shock does not separate the flow near the viscous separation point. The experimental data show two separations—primary at $\theta = 120.3$ deg and secondary at 160 deg, while the inviscid separation is at $\theta = 151.3$ deg. The longer plateau in pressure in the experiment behind the primary separation point is due to the secondary separation; otherwise, the Euler and experimental pressure distributions would be similar. It is the expansion and recompression of the reverse flow that causes secondary separation. It should be clear that while the vorticity produced by the cross-flow shock is not the whole separation story, it may play an important role in the process. There are two sources of vorticity in this flowfield—the shock and the boundary layer. Both of these sources of vorticity play a role in separation and the resulting spiral or vortex.

Summary of Findings and Future Work

This study has found that the vorticity produced by a cross-flow shock present in the supersonic flow about cones at high incidence can cause separation and spiraling. A number of important features of these solutions were shown.

1) An independence of these solutions to any numerical artifices; that is, artificial viscosity (truncation error), captured shocks, or initial conditions.

2) Why the conceptual problem associated with the two-dimensional closed-separation bubbles does not exist in conical flow. Since no closed-recirculation zones exist in the conical flow, all quantities transmitted along streamlines can be uniquely defined.

3) The variation of shock-induced separation location with shock strength (Fig. 12), indicating the possibility that the spiral is eliminated before the cross-flow shock.

4) The development of a second reverse cross-flow shock (Figs. 14 and 15) with the possibility of shock-induced secondary separation.

It should be obvious that any computation that relies on the potential flow approximation alone cannot predict these flowfields. While the shock-induced vorticity may play an important role in viscous separation, it is by no means the whole picture (see Fig. 16).

This work has uncovered as many problems as it has solved. The somewhat surprising behavior of the lee plane saddle/node combination once the spiral appears must be studied in detail. The saddle/node combination (Figs. 9 and 10) that is present at subcritical α's and remains with weak spirals is eliminated as the spiral gets larger (Figs. 4 and 5). The possibility of a second reverse shock (Fig. 15) causing secondary separation is an interesting possibility that must be investigated.

Acknowledgments

The author gratefully express his appreciation to Dr. A. Rubel for his many helpful discussions during the course of this work and Dr. M. Siclari for supplying the full potential calculations. Both are from Grumman's Research and Development Center.

References

[1] Rao, D.M., "Vortical Flow Management for Improved Configuration Aerodynamics—Recent Experiences," AGARD CP-342, 1983, pp. 30-1-30-14.

[2] Küchemann, D. "Inviscid Shear Flow Near the Trailing Edge of an Aerofoil," RAE TR 67068, 1967.

[3] Frankel, L.E., "On Corner Eddies in Plane Inviscid Shear Flow," *Journal of Fluid Mechanics,* Vol. 11, 1961, pp. 400-406.

[4] Smith, P.D., "A Note on the Computation of the Inviscid Rotational Flow Past the Trailing Edge of an Airfoil," RAE TM 1217, 1970.

[5] Salas, M.D., "Recent Developments in Transonic Euler Flow Over a Circular Cylinder," NASA TM 83282, 1982.

[6] Schmidt, W. and Jameson, A., "Recent Developments in Finite Volume Time-Dependent Techniques for Two and Three Dimensional Transonic Flows," in *Computational Fluid Dynamics,* Lecture Series Notes 1982-04, VKE, Brussels, 1982.

[7] Hornung, H.G., "The Vortex Skeleton Model for Three-Dimensional Steady Flows," AGARD CP-342, 1983, pp. 2-1-2-12.

[8] Smith, J.H.B., "Remarks on the Structure of Conical Flow," *Progress in Aeronautical Sciences,* Vol. 12, 1972, pp. 241-271.

[9] Smith, J.H.B., "Behavior of a Vortex Sheet Separating from a Smooth Surface," RAE TR 77058, 1977.

[10] Smith, F.T., "Three-Dimensional Viscous and Inviscid Separation of a Vortex Sheet from a Smooth Non-Slender Body," RAE TR 78097, 1978.

[11] Fiddes, S.F., "A Theory of the Separated Flow Past a Slender Cone at Incidence," AGARD CP 291, 1981, pp. 30-1-30-14.

[12] Marconi, F., "The Spiral Singularity in the Supersonic Inviscid Flow Over a Cone," AIAA Paper 83-1665, July 1983.

[13] Bryson, A.E., "Symmetric Vortex Separation on Circular Cylinders and Cones," *Journal of Applied Mechanics,* Vol. 81, Dec. 1959, pp. 643-648.

[14] Rizzi, A., Ericksson, L., Schmidt, W., and Hitzel, S., "Numerical Solutions of the Euler Equations Simulating Vortex Flows Around Wings," AGARD CP-342, 1983, pp. 21-1-21-14.

[15] Nielsen, J.N., Kuhn, G.D., and Klopfer, G.H., "Euler Solutions of Supersonic Wing-Body Interference at High Incidence Including Vortex Effects," NEAR TR 263, 1982.

[16] Marconi, F., "Supersonic Inviscid, Conical Corner Flow Fields," *AIAA Journal,* Vol. 18, Jan. 1980, pp. 78-84.

[17] Moretti, G., "The λ-Scheme," *Computers and Fields,* Vol. 7, 1979, pp. 191-205.

[18] Marconi, F., Salas, M.D., and Yaeger, L., "Development of a Computer Code for Calculating the Steady Super/Hypersonic Inviscid Flow Around Real Configurations," NASA CR-2675, 1976.

[19] Rudman, S., "Multinozzle Plume Flow Fields—Structure and Numerical Calculations," AIAA Paper 77-710, June 1977.

[20] deNeef, T. and Moretti, G., "Shock Fitting for Everybody," *Computers and Fluids,* Vol. 8, 1980, pp. 327-334.

[21] Siclari, J.M., "Investigation of Cross Flow Shocks on Delta Wings in Supersonic Flow," AIAA Paper 79-0345, Jan. 1979.

[22] Peake, D.J., Fisher, D.F., and McRae, D.S., "Flight, Wind Tunnel and Numerical Eperiments with a Slender Cone at Incidence," *AIAA Journal,* Vol. 20, Oct. 1982, pp. 1338-1345.

[23] Rubel, A., "Inviscid Axisymmetric Jet Impingement with Recirculating Stagnation Regions," *AIAA Journal,* Vol. 21, March 1983, pp. 351-357.

[24] Vorropoulos, G. and Wendt, J.F., "Laser Velocimetry Study of Compressibility Effects on the Flow Field of a Delta Wing," AGARD CP-342, 1983, pp. 9-1-9-13.

[25] Rainbird, W.J., "The External Flow Field About Yawed Circular Cones," AGARD CP 30, 1968, pp. 19-1-19-18.